



Critical role of the light spectrum on the simulation of solar photocatalytic reactors

Cintia Casado, Ángela García-Gil, Rafael van Grieken, Javier Marugán*

Department of Chemical and Environmental Technology, ESCET, Universidad Rey Juan Carlos, C/ Tulipán s/n, 28933, Móstoles, Madrid, Spain



ARTICLE INFO

Keywords:
 Solar light
 Spectral distribution
 Photoreactor
 Photocatalysis
 Water treatment
 CFD modelling

ABSTRACT

This work describes the critical role of the matching between the spectral distribution of the incident light and the absorption spectra of the semiconductor material on the accuracy of the simulation of solar photocatalytic reactors. In silico results have been generated by a multiphysics model including the rigorous description of the hydrodynamics, radiation transfer, mass transport and chemical reaction rate, with the particular feature of using a spectral band discretization approach for the resolution of the radiation balance and the estimation of the spectral local volumetric rate of photon absorption. Model predictions with a mechanistic kinetic model have been experimentally validated using a solar reactor based on a tubular reactor coupled to a compound parabolic collector (CPC) under illumination with a solar simulator (xenon lamp) and natural sunlight. Small differences in the spectral distribution of both light sources led to significantly different predictions for the reaction rate, explaining the higher efficiency experimentally achieved with natural sunlight in comparison with the solar simulator for equivalent total UV-A irradiances. The developed model is able to explain the discrepancies between experimental results in solar simulators and under natural sunlight, usually reported in the literature, offering a novel numerical approach for rigorous modelling of photoreactors using light sources with any spectral distribution.

1. Introduction

The use of sunlight to activate photocatalytic processes has huge potential both from an environmental and economic point of view. This technology has been demonstrated to be effective for several applications, such as water and air decontamination and disinfection or industrial production of fine chemicals [1]. However, the high variability of irradiation power and solar spectrum, depending on latitude, longitude, date, time, pollution and meteorological conditions means that the efficiency of solar processes depends to a large extent on the availability of resources [2] (and therefore the cost).

Compound parabolic collectors photoreactors (CPCs-PR) are the most promising non-concentrating solar reactors, considered to be the most efficient and mature design in photochemical applications [2,3]. This kind of photoreactor has been widely used in pilot-scale and demonstration plants with collector areas ranging from 3 m² to even 150 m² [1].

The modelling of solar photocatalytic reactors can contribute to the increase in their efficiency, identifying improvements in the design or assisting in the scaling-up process. The most complex task in photoreactor modelling is the resolution of the radiation field and its

integration in the kinetic equation. The use of computational numerical modelling tools has been proved to be an efficient approach on this purpose [4–7]. These tools are based on a discretization scheme that allows the resolution in complex geometries of rigorous calculations of the radiative transport equation (RTE) in absorbing and scattering media, coupled to the hydrodynamics, radiation transfer, mass transport and chemical reaction rate within the reactor.

From the different methods reported in the literature to describe the radiation field of CPCs-PR [8–13], the finite volume-based numerical simulation is the best way to integrate all physical phenomena, including the rigorous resolution of the RTE, in 3D simulations. Ren et al. [14] published in 2016 the only existing report on the finite volume simulation of tubular reactors combined with CPC, including the modelling of hydrodynamics and radiation absorption. However, these authors used a simplified radiation model based on a modified differential approximation of P1 method in 2D, and a kinetic model of the chemical reaction was not integrated in the simulation.

As in any other chemical reactor, the modelling of photocatalytic reactors requires first the knowledge of the kinetics of the involved chemical process. In order to have predictive capacity beyond the limits of operation in which the kinetic parameters have been obtained, the

* Corresponding author.

E-mail address: javier.marugan@urjc.es (J. Marugán).

model must have a mechanistic character, using intrinsic kinetic parameters with a well-defined physical meaning. In a previous work [4], a rigorous kinetic model was proposed for the photocatalytic oxidation of methanol to formaldehyde, and the intrinsic kinetic parameters were obtained under optically differential conditions. The kinetic model and parameters were satisfactory applied to the numerical modelling of a slurry annular photoreactor illuminated with a 365 nm wavelength fluorescent lamp with titanium dioxide used as photocatalyst. In the present work, the developed kinetic model and methodological approach was used for the first time to simulate CPC solar photoreactors illuminated both with solar simulated light (xenon lamp) and with natural sunlight. Predictive results for different TiO_2 concentrations and light conditions were validated with experimental data. A novel method for considering the spectral distribution of the solar light is here presented. The RTE has been solved for different wavelength ranges, which allowed the incorporation not only of the spectral features of the incident light, but also of the spectral dependence of the radiation absorption by the TiO_2 . For the simulation of reactors operating with natural solar radiation, the solar vector describing the directional dependence of the incident irradiation was calculated and it was coupled with the radiation transport within the reactor. The present work will show how this rigorous approach to the modelling of the solar light considering the directional and spectral features allows to explain the significant differences in the process efficiency achieved under real sunlight in comparison with the use of a solar simulator with equivalent global UV-A irradiance.

2. Experimental methods

2.1. Photocatalytic reactor

The CPC-PR is a tubular reactor coupled to a CPC reflector that can be used either with a solar simulator (xenon lamp, XBO 5000 W / H XL OFR, 6000 K) or under natural sunlight. The reactor consists of a borosilicate glass tube with an inner diameter of 26 mm and a length of 380 mm located on the focal axis of the CPC, being the irradiated volume 0.2 L. The total working volume is 1 L, being the water recirculated from a reservoir tank by a centrifugal pump with a flow rate of $12.3 \text{ L} \cdot \text{min}^{-1}$. The surface of the reflector is made of anodised aluminium and due to its double parabolic geometry guarantees an 85% direct light reflection towards the central pipe. For experiments with artificial light, the collector surface was placed perpendicular to the direction of the light, whereas experiments with natural sunlight were carried out using an inclination of 40°, corresponding to the local latitude of Universidad Rey Juan Carlos facilities in Móstoles, Spain (40.33° N, 3.86° W). A schematic representation of the experimental set-up can be found elsewhere [15].

2.2. Reaction procedure

Photocatalytic experiments were carried out using Evonik P25 TiO_2 as semiconductor material in suspension, with loadings in the range from 0.02 to 0.1 g L^{-1} and different irradiation conditions. The evaluation of the reaction efficiency was done by means of photocatalytic oxidation of methanol to formaldehyde. This test reaction has been extensively studied in previous research works, being available in the literature the parameters of a mechanistic kinetic model with explicit radiation absorption effects [4]. The progress of the reaction was quantified by following the formation of formaldehyde, quantitative oxidation product when methanol is in excess [16]. More details of the reaction procedure and formaldehyde analysis can be founded elsewhere [4].

3. Computational model

3.1. Geometry and mesh

The CPC-PR model consist of three domains (Fig. 1A): the tubular reactor itself; the transparent tube that delimits it; and the air space between the reactor and the CPC specular reflector that defines the geometry of the model. To reduce the calculation time, a boundary condition has been established at the frontal collection area. The mesh optimized for this reactor has 585556 cells, with an average cell volume of 4 mm^3 . This cell density was proven to be high enough to ensure mesh-independent results. Due to the curvature of the reflector, the meshing in the air domain is mostly tetrahedral, as this type of cells allows a simpler adaptation on curved surfaces. Due to the simplicity of the tubular photoreactor geometry, a mesh with hexahedral cells has been used to reduce the number of total cells of the model.

3.2. Radiation model

For the modelling of the radiation field, the radiative transfer equation (RTE, Eq. 1) was solved, taking into account for a specific direction the energy loss due to absorption and out-scattering and energy gain due to in-scattering from other different directions.

$$\frac{dI_{\lambda,\Omega}}{ds} = -\kappa_{\lambda} I_{\lambda,\Omega} - \sigma_{\lambda} I_{\lambda,\Omega} + \frac{\sigma_{\lambda}}{4\pi} \int_{\Omega'=4\pi} p(\Omega' \rightarrow \Omega) I_{\lambda,\Omega'} d\Omega' \quad (1)$$

To solve this equation, the spectral dependence of the volumetric absorption coefficient κ_{λ} , the volumetric scattering coefficient σ_{λ} and the phase function that describes the directional distribution of scattered radiation $p(\Omega' \rightarrow \Omega)$ were required. The result of the equation provides the intensity of photons with wavelength λ propagated along direction Ω , $I_{\lambda,\Omega}$. The integral of this equation above all the spatial directions allows the evaluation of the radiation field at any point inside the reactor space, and the local volumetric rate of energy absorption (VREA) can be calculated multiplying this value by the absorption coefficient.

The numerical resolution of the RTE was carried out using the *Discrete Ordinate Method* (DOM) available in ANSYS® Fluent software. This method solves the RTE for a finite number of discrete solid angles, also called control angles, result of the discretization of the sphere octant in $N_{\theta} \times N_{\phi}$ solid angles. Each solid angle is associated with a direction vector for the directional discretization of the RTE. The selection of the angular discretization must be carefully studied for each modelled emission source, since, together with an adequate mesh density, must be enough to correctly capture the shape of the emission. In the simulations presented in this work, a discretisation of 15×15 was used. In order to simplify the computational model, the coupling of the radiation balance with the overall energy balance of the system was avoided, annulling the thermal emission by establishing a value of temperature of 1 K in all regions and walls of the model.

3.2.1. Spectral bands model

As described in Section 2.1 the CPC-PR has been used both illuminated by a solar simulator, and with natural sunlight. The spectral distribution of both light sources in the UV range is represented in Fig. 1B, together with the wavelength dependence of the specific absorption coefficient of P25 TiO_2 suspensions [17]. Although the solar simulator has been designed to reproduce the standard solar spectra in the whole UV-vis range, it can be observed that some differences appear when the UV-A range is analysed in detail. These differences could have a significant impact on the results, as the absorption of the catalyst is higher for short wavelength, where less photons are available. In contrast, the absorption decreases significantly for wavelength values close to the visible range, where the available radiation is higher. The rigorous modelling of this uneven distribution of the emission/absorption requires a fine spectral discretization of the radiation transport

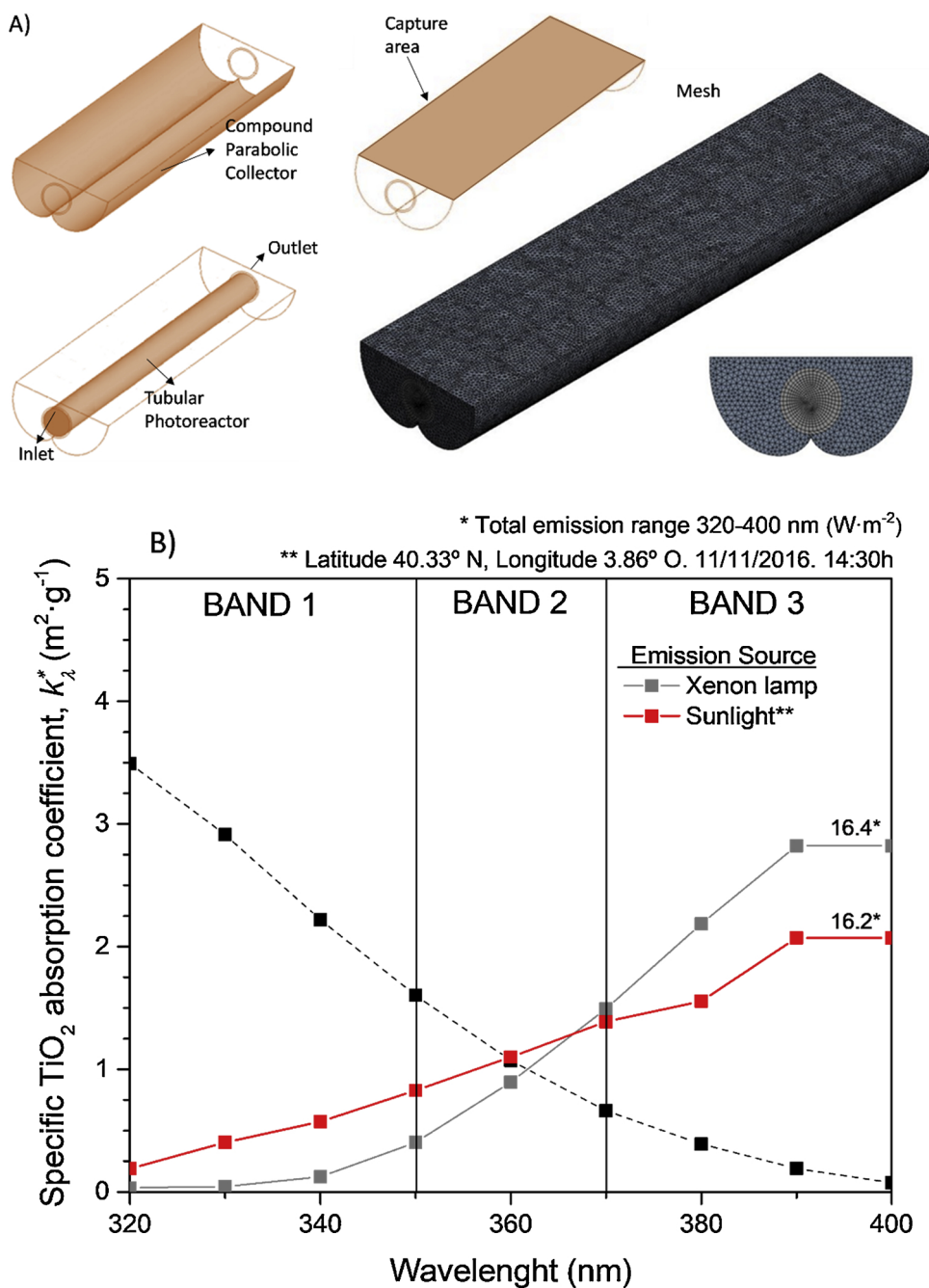


Fig. 1. A) Modelled geometry and mesh for the tubular photoreactor coupled to a compound parabolic collector. B) Specific absorption coefficient of TiO_2 P25 for different wavelengths, and spectral distribution of the emission of the xenon lamp and the sunlight experimentally determined a random day in the location of the Waste Water Treatment Plant facilities at Rey Juan Carlos University, in Móstoles, Spain (40.33° N, 3.86° W).

that leads to a huge computational cost. Therefore, average values for the whole UV-A range are usually assumed for modelling purposes [8,18,19]. This work presents an intermediate approach, splitting the UV-A range into different spectral bands in which the emission/absorption properties are significantly different. Fig. 1B shows the three spectral bands considered, assuming average properties of the emission and absorption coefficients inside each band.

For the calculation of radiation scattering, the Henyey and Greenstein phase function was included in the model as a subprogram (User Defined Function, UDF), using an averaged value for the UV-A range of $g_\lambda = 0.528$ [17]. The volumetric absorption and scattering coefficients ($\text{in } m^{-1}$) were calculated by multiplying the corresponding specific values by the mass loading of catalyst (C_{cat} , in $\text{g} \cdot \text{m}^{-3}$).

In all spectral bands, air was considered as non-participating media (absorption and scattering coefficients equal to zero) and the CPC was simulated as a specular reflecting surface with 85% reflectance. The rest of the walls, except the collection area, have been considered transparent, specified in ANSYS® Fluent as semi-transparent wall with the absorption and emission values set to zero.

3.2.2. Modelling the xenon lamp (solar simulator)

The xenon lamp used in the CPC-PR is placed 2 m away from the collector. To avoid unnecessary computational costs, the model does not simulate the emission from the lamp, but uses as a boundary condition the incident UV radiation experimentally determined in the collection area (Fig. 1A) and whose value can be controlled. The CPC-

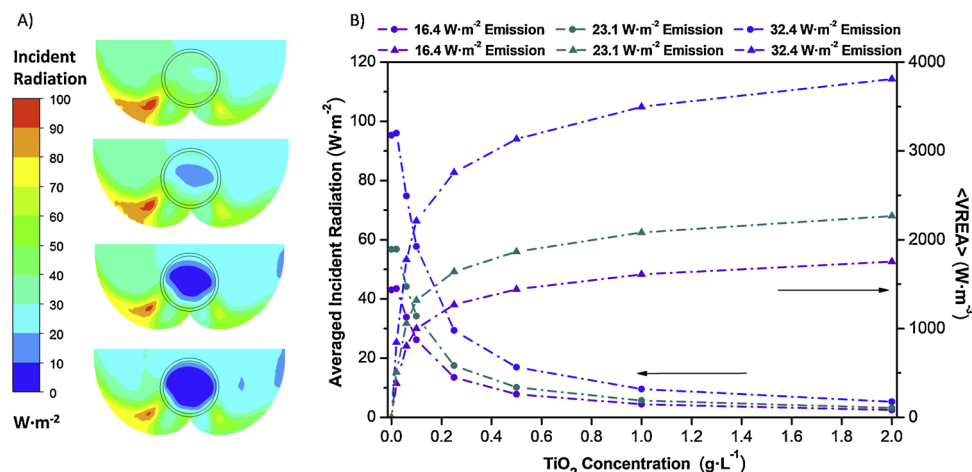


Fig. 2. A) Incident radiation in the central plane of the CPC-PR for an incident radiation of $16.4 \text{ W}\cdot\text{m}^{-2}$ and different TiO_2 concentrations (from top to bottom): $0.06 \text{ g}\cdot\text{L}^{-1}$, $0.1 \text{ g}\cdot\text{L}^{-1}$, $0.25 \text{ g}\cdot\text{L}^{-1}$ and $0.5 \text{ g}\cdot\text{L}^{-1}$. B) Volume averaged incident radiation and VREA in the CPC-PR.

PR is not centred with the emission cone of the xenon lamp, but shifted towards the bottom, and this effect has been considered in the simulation. The averaged values of incident radiation in the collection area used in this work were $16.4 \text{ W}\cdot\text{m}^{-2}$, $23.1 \text{ W}\cdot\text{m}^{-2}$ and $32.4 \text{ W}\cdot\text{m}^{-2}$. The direction of incident radiation was considered normal to the boundary.

3.2.3. Modelling the solar radiation

ANSYS® Fluent Solar Calculator was used to compute the solar vector during the experiments carried out at the facilities of the Technological Support Centre at the Rey Juan Carlos University, Spain (40.33°N , 3.86°W). This tool uses the calculations provided by the National Renewable Energy Laboratory (NREL, USA) [20], having enough precision for photocatalytic applications [2], and allowing the estimation of the solar conditions for different geographical locations [21]. It provides an estimation of the direct and diffuse solar radiation and therefore the distribution of directions of the incident radiation, that can be coupled to the DOM algorithm used to solve the radiation transport. Although the total irradiance can be also estimated through the software, the computational cost of the model has been reduced introducing as boundary condition the UV irradiance values experimentally determined by radiometry, using a StellarNet Spectrometer Blue-wave UVIS-25 (329–400 nm) calibrated equipment.

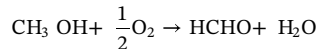
3.3. Fluid-dynamics, photochemical reaction and species mass transport modelling

The photoreactor simulation requires the resolution of the mass balances of each species in a non-stationary state including not only mass transfer by diffusion and advection mechanisms but also the chemical reaction term. The equation of the mass conservation taking into account the diffusive flux, the reaction rate and the coupling with the hydrodynamics calculations was described in a previous publication [4]. The simulation of the fluid dynamics was performed considering a three dimensional, steady state, and pseudo-homogeneous behaviour using the standard $k\text{-}\epsilon$ turbulence model, the most adopted turbulence model for photocatalytic reactors [22], and whose equations can be founded elsewhere [23].

The physical properties of water have been used, and the fluid has been established as Newtonian, incompressible, and isothermal with constant physical properties. The flow rate of the reactor was measured experimentally ($12.3 \text{ L}\cdot\text{min}^{-1}$, Reynolds number of 10140), and the calculated velocity corresponding to the reactor inlet surface ($0.385 \text{ m}\cdot\text{s}^{-1}$) was used in the computational model. In the outlet boundary, the atmospheric pressure value has been set. The walls have been set as static, without roughness. The standard wall function was

used, based on the logarithmic proposal of Launder and Spalding [24], commonly used in engineering.

The description of the reaction rate was carried out by means of a kinetic model previously developed [4]. This model describes the kinetics of the photocatalytic oxidation of methanol based on a mechanistic description of the process including explicitly the radiation absorption step, charge transfer and radical propagation. Its intrinsic kinetic parameters, calculated from experiments in an optically different photoreactor, allow the application of the model to different geometries, hydrodynamic and optical conditions. Considering the global stoichiometry of the reaction as:



The rate of formaldehyde formation when methanol is in a large excess can be represented by Eq. 2:

$$r_{\text{HCHO}} = \alpha_1(-1 + \sqrt{1 + \alpha_2 \cdot e^a}) \quad (2)$$

Under low irradiation conditions it can be assumed that $\alpha_2 \cdot e^a \ll 1$, taking the first term of the Taylor expansion of the square root, Eq. 2 will take the form:

$$r_{\text{HCHO}} = \alpha \cdot e^a \quad (3)$$

where the formaldehyde production rate (r_{HCHO} , $\text{kmol}\cdot\text{m}^{-3}\cdot\text{s}^{-1}$) can be reasonably described as proportional to the VREA (e^a , $\text{W}\cdot\text{m}^{-3}$). The values of the kinetic parameters are $\alpha = 3.17 \pm 0.22 \times 10^{-10} \text{ kmol}\cdot\text{W}^{-1}\cdot\text{s}^{-1}$, $\alpha_1 = 5.12 \cdot 10^{-7} \pm 210 \text{ kmol}\cdot\text{m}^{-3}\cdot\text{s}^{-1}$, $\alpha_2 = 1.13 \pm 5.10 \times 10^{-3} \text{ m}^3\cdot\text{W}^{-1}$ [4].

The simulations of the photocatalytic reaction have been carried out in a non-stationary state. The time step was established at 1 s, low enough to provide stable simulation results. The initial mass fractions of methanol and oxygen used were $3.2 \cdot 10^{-3}$ g/g and $9.1 \cdot 10^{-6}$ g/g respectively, corresponding to 0.1 M CH_3OH and to the concentration of maximum solubility of air in water at 25°C . The values of the diffusion coefficients used for the different species were estimated using the database of the commercial software Aspen Plus® $D_{(\text{HCOH}, \text{m})} = 1.78 \cdot 10^{-9} \text{ m}^2\cdot\text{s}^{-1}$, $D_{(\text{O}_2, \text{m})} = 2.088 \cdot 10^{-9} \text{ m}^2\cdot\text{s}^{-1}$, $D_{(\text{CH}_3\text{OH}, \text{m})} = 1.62 \cdot 10^{-9} \text{ m}^2\cdot\text{s}^{-1}$ y $D_{(\text{H}_2\text{O}, \text{m})} = 1.78 \cdot 10^{-8} \text{ m}^2\cdot\text{s}^{-1}$.

The modelling of the recirculation, dilution and mixing of the reactor outlet in the reservoir tank was also introduced in the model by a subprogram code (UDF) according to Eq. (4):

$$Y_i = \frac{Y_{i\text{out}} \cdot \Delta t + \tau \cdot Y_{i\text{in}}}{\Delta t + ST} \quad (4)$$

where Y_i is the inlet fraction of species every time step, ST is the space time in the reservoir tank and Δt is the time step (1 s).

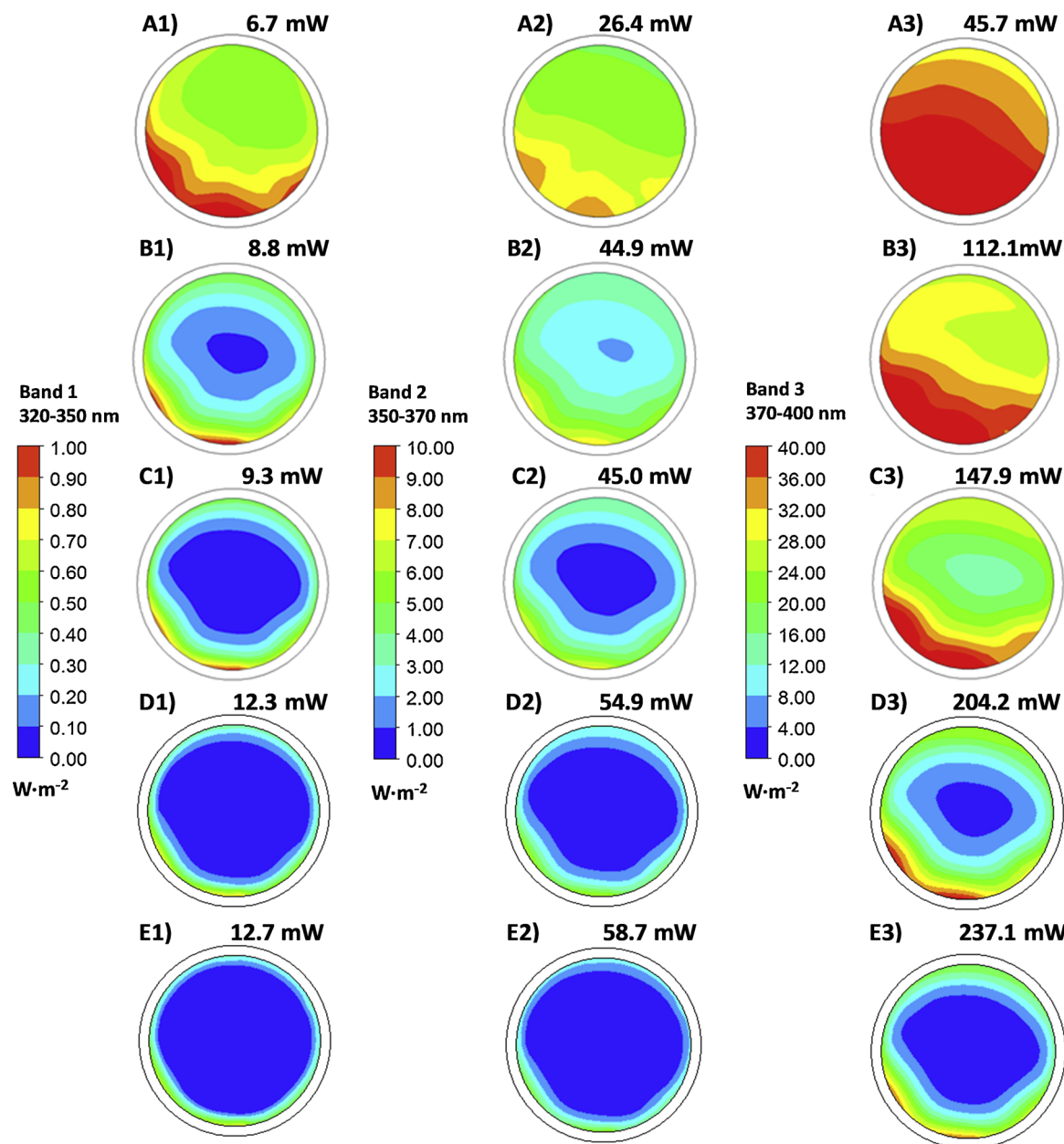


Fig. 3. Incident radiation for each emission / absorption band in the central plane of the reactor tube, for a radiation emitted of $16.4 \text{ W} \cdot \text{m}^{-2}$ and different TiO_2 concentrations: A) $0.02 \text{ g} \cdot \text{L}^{-1}$, B) $0.06 \text{ g} \cdot \text{L}^{-1}$, C) $0.1 \text{ g} \cdot \text{L}^{-1}$, D) $0.25 \text{ g} \cdot \text{L}^{-1}$ and E) $0.5 \text{ g} \cdot \text{L}^{-1}$. The numbers on the images indicate the energy absorbed in each band (mW).

3.4. Convergence criteria and solution strategy

The discretization scheme was set as second order upwind, the standard method was selected for pressure. The SIMPLE algorithm was chosen for the pressure–velocity coupling. Convergence of the numerical solution was ensured by monitoring the scaled residuals to a criterion of at least 10^{-6} for the momentum variables, continuity and incident radiation, and $5 \cdot 10^{-4}$ for the concentrations. Additionally, the variables of interest have been monitored at different surfaces of the computational domain as indicator of convergence (at least 50 iterations without changes).

4. Results

4.1. Artificial lighting: radiation field

The effect of the TiO_2 catalyst loading was first studied. The results

of the calculation of the global radiation field totalizing the absorption and scattering of the different spectral bands (Fig. 2A) show that above $0.25 \text{ g} \cdot \text{L}^{-1}$ most of the absorption takes place in the outer zone of the tube, whereas inner part of the tube is almost in the dark, causing that the average VREA inside the reactor hardly varies above $0.25 \text{ g} \cdot \text{L}^{-1}$. The asymmetry in the contour plots is due to the position of the CPC in the illumination cone of the xenon lamp. Fig. 2B shows the total absorbed energy obtained with the spectral bands model as a function of the catalyst concentration, showing an optimum catalyst loading for $0.25 \text{ g} \cdot \text{L}^{-1}$ of TiO_2 . Above this value, the increase in the average absorption is no longer proportional, requiring a much higher amount of catalyst to get a relatively small increase in the absorption of radiation. This optimum, estimated for the use of solar simulator artificial lighting, is not necessarily the same for the use of real solar light or any other different lighting system, as it would vary depending on the spectrum of the emitted radiation.

The total energy absorbed along the reactor radius has been

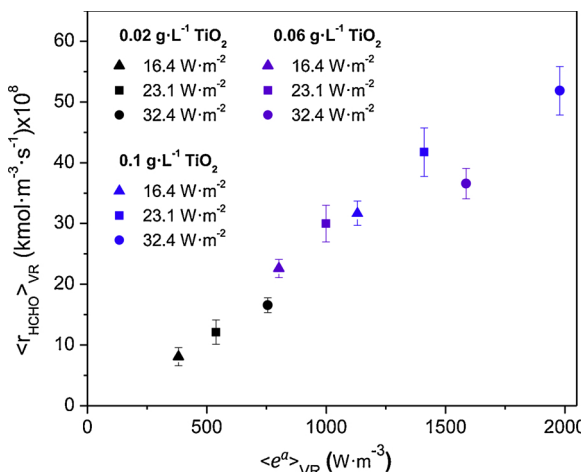


Fig. 4. Experimental reaction rates for formaldehyde production obtained in the CPC-PR under different lighting conditions and photocatalyst concentration.

calculated as the sum for the three spectral bands of the product of the incident energy multiplied by the corresponding absorption coefficient, which varies with the TiO_2 concentration. As expected, the absorbed energy increases with the catalyst loading for the three intensities of UV irradiation studied. Colina-Márquez et al. [8], reported for a CPC with a tube 3.3 cm in diameter, an optimum concentration of P25 TiO_2 of 0.21 g L^{-1} , in line with previous results [25,26], and with those presented in this research for a similar tube diameter (2.6 cm).

The representation of the absorbed energy in the central plane of the interior of the reactor tube for each spectral band is shown in Fig. 3. The energy emitted by the lamp between 320 and 350 nm is almost completely absorbed by the catalyst for a concentration of 0.1 g L^{-1} (Fig. 3C1), as the emission in this interval of wavelength is the lowest and the absorption the highest. The complete absorption of the energy

emitted in the second spectral band, between 350 and 370 nm, takes place at a higher concentration of 0.25 g L^{-1} (Fig. 3D2). Finally, although the TiO_2 absorption is quite low for the spectral range between 370–400 nm, the high emission of the lamp in this interval explains that the highest contribution to the total absorption is, by far, due to this spectral band, which is not completely absorbed until a concentration of TiO_2 of 0.5 g L^{-1} (Fig. 3E3). For this concentration, all the energy emitted by the lamp in the whole spectrum can be considered to be absorbed.

4.2. Artificial lighting: photocatalytic activity

Experiments of photocatalytic oxidation of methanol were carried out at three different values of the UV-A incident radiation (16.4 W m^{-2} , 23.1 W m^{-2} and 32.4 W m^{-2}) and for three TiO_2 concentrations. The values of the reaction rates of formaldehyde formation versus the calculated averaged VREA in the reactor are represented in Fig. 4. As expected, for the same catalyst concentration the experimental reaction rates increase as the incident radiation does, and higher values are also obtained increasing the catalyst concentration. In this experimental range, the dependence of the reaction rate on the VREA is clearly linear, as it could be anticipated by the values calculated for the radial distribution of $\alpha_2 \cdot e^a$, mostly lower than 1, and there supporting the used of the simplified kinetic model in its version for low irradiation (Eq. (3), described in Section 3.3).

Fig. 5 shows the comparison between the experimental data and the results of the prediction of formaldehyde production resulting from the computational model using the kinetic model represented in Eq. (3). The simulations of the transient photochemical reaction were based on the calculated radiation field and the fluid mechanic simulation of the reactor described in a previous work [21]. As it can be seen in the Fig. 5A–C, the spectral bands CFD model has been able to predict with good accuracy the photocatalytic activity of the reactor in the nine experimental combinations of irradiance and catalysts concentration employed, being the error inside the experimental range for most of the

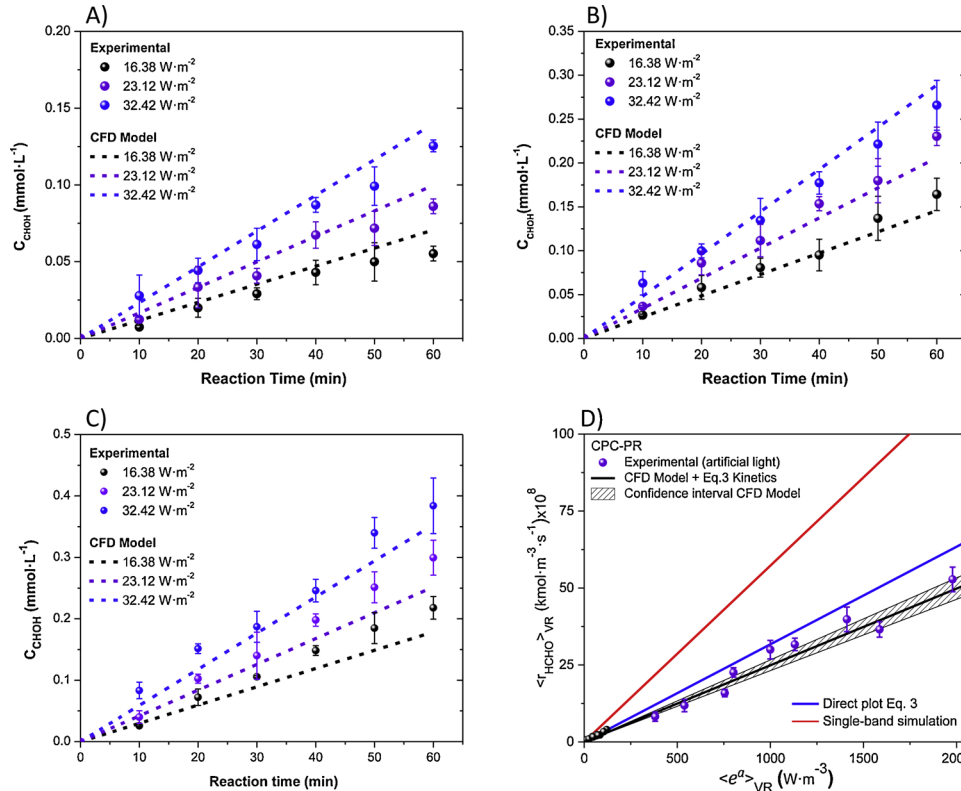


Fig. 5. Experimental results and predicted by the CFD model based on the proposed kinetic model in its version for low irradiation, and the obtained intrinsic kinetic parameters, for different TiO_2 concentrations: A) 0.02 g L^{-1} , B) 0.06 g L^{-1} and C) 0.1 g L^{-1} . D) Comparison of experimental reaction rates of formaldehyde formation obtained in the CPC-PR and predicted by the CFD model, for different absorbed energy conditions.

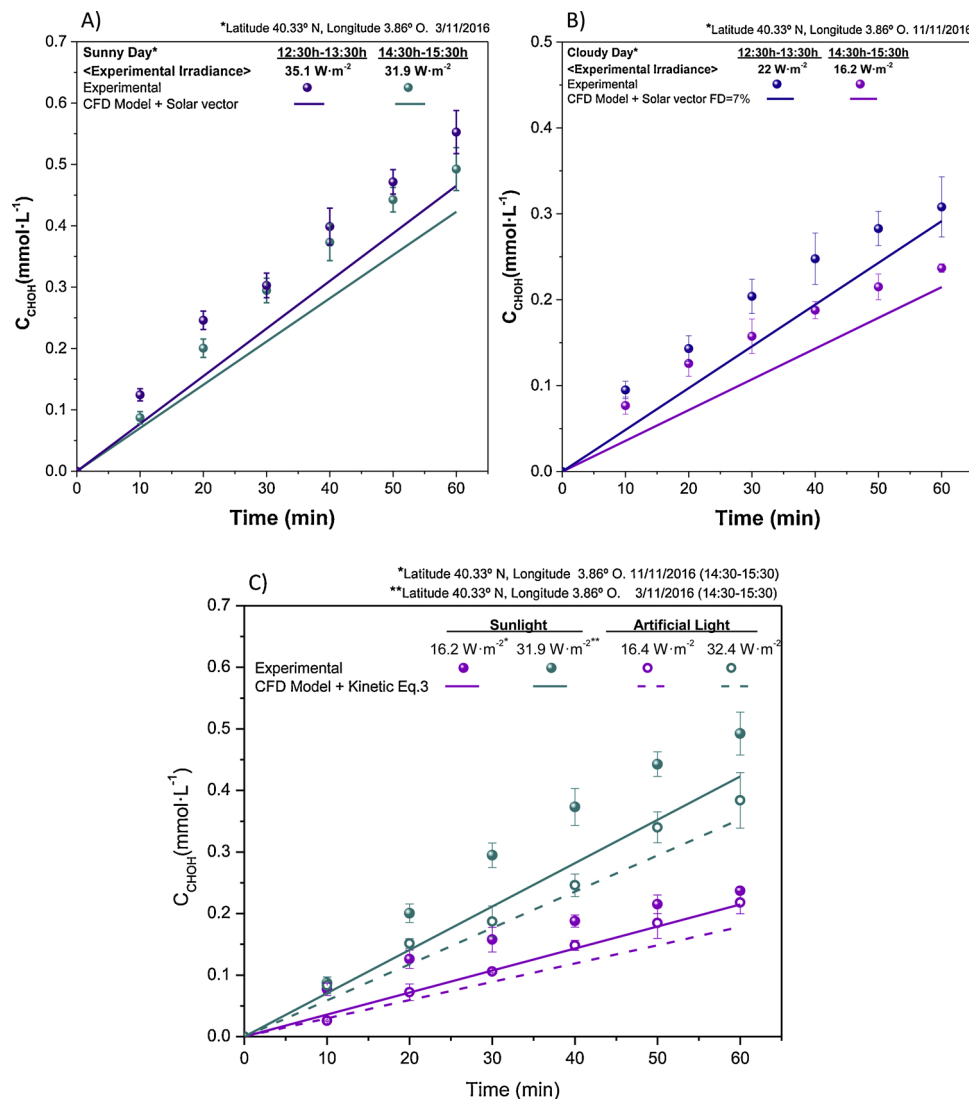


Fig. 6. Experimental results and prediction of the CFD model with the kinetic model for low irradiance using the solar incident radiation value calculated with the Fair Weather Conditions method and measured experimentally. A) for a sunny day, B) for a cloudy day. C) Experimental results and prediction when the reactor is illuminated with artificial light and sunlight.

data. Fig. 5D shows how the values of the experimental reaction rates are mostly inside the 95% confidence level of the prediction of the CFD model in the whole range of values of VREA. It can be observed that for higher values of TiO₂ concentration, the differences between the use of an averaged VREA value (direct plot of Eq. (3), blue line) and the result of the resolution of the differential equations in each cell of the reactor become more significant. This error is dramatically higher if, instead of using the spectral bands model, a single spectral band simulation with average radiation properties in the whole UV-A range from 320 to 400 nm is carried out. In this case, the reaction rates would be clearly overestimated, with values in the order of 2.3 times higher than the experimental data (Fig. 5D, red line). Consequently, the use of the computational model, and especially the spectral bands features, are proven to be able to accurately predict the experimental results, showing the utility of the global methodology proposed in the modelling of photocatalytic reactors, and specifically for applications based on the latest LED light sources [27,28]. Similarly, this methodology could be easily extrapolated to any other photocatalyst, including those active in the visible range of the spectrum, just recording the action spectra in the specific wavelength range in which the material absorbs radiation.

4.3. Photocatalytic activity under sunlight

Experimental runs with the CPC-PR reactor using natural sunlight were carried out using 0.1 g·L⁻¹ of TiO₂ in days and hours with different solar irradiance during the month of November 2016. The simulations of the reactions have been carried out using the experimental value of solar incident radiation, measured with a spectroradiometer, and introduced into the model together with the position of the solar vector resulting from the Solar Calculator. In each case, the emission contribution of each band of the model has been calculated from the spectral distribution of the solar irradiance.

The simulation provides reasonable results for the prediction of the reaction evolution with a clear sky, as it can be seen in Fig. 6A. In contrast, for reactions on cloudy days (Fig. 6B), the model is not able to take into account the changes in the irradiance causing that the reaction rate varies with time, leading to a non-linear production of formaldehyde. Even though the simulations with the average radiation have been satisfactorily closer to the experimental values, non-stationary simulations, in which the incident radiation is updated as a function of time, would be necessary for more accurate predictions. Future efforts to improve solar photoreactors modelling should be devoted to this goal.

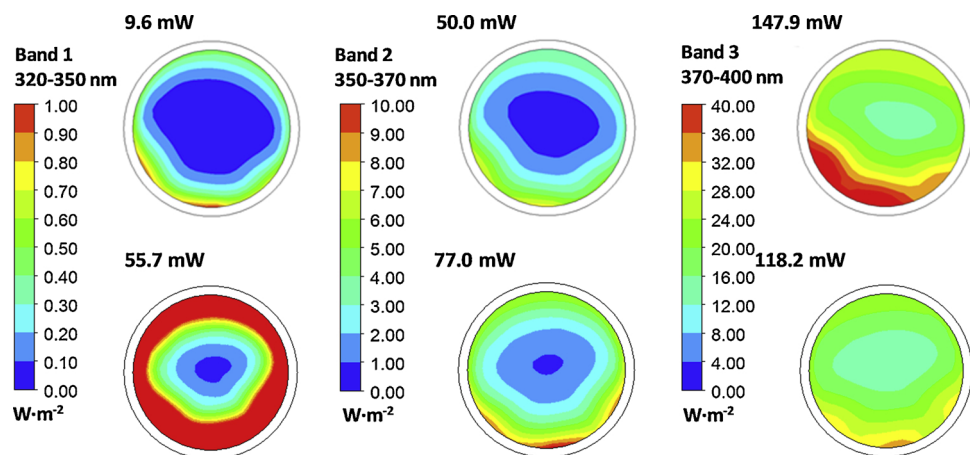


Fig. 7. Incident radiation for each emission / absorption band in the central plane of the CPC-PR, with a TiO_2 concentration of 0.1 g L^{-1} and different sources of radiation. Up: Xenon solar simulator 16.4 W m^{-2} , Down: Solar light 16.2 W m^{-2} . The numbers on the images indicate the energy absorbed in each band (mW).

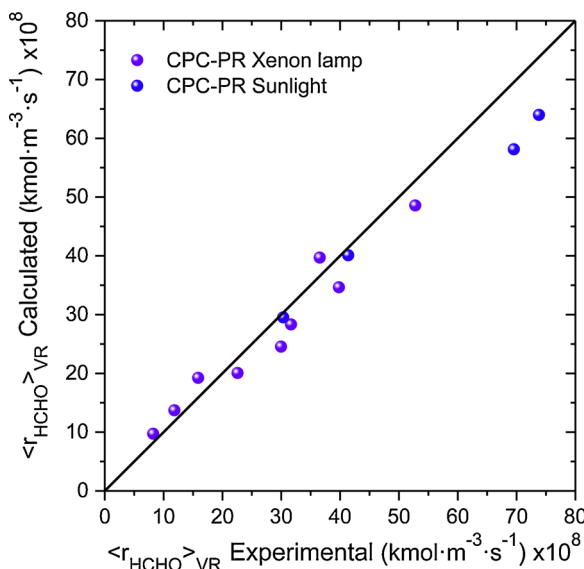


Fig. 8. Predicted versus experimental reaction rates in all the studied conditions.

Fig. 6C shows the comparison of the experimental results for the CPC-PR, under natural and artificial solar light (xenon lamp) for similar experimental irradiance conditions around 16 and 32 W m^{-2} of UV-A. As it can be observed, the photocatalytic activity for comparable global UV-A irradiance is much higher under natural sunlight conditions, what is certainly due to the small differences in the light spectra shown in **Fig. 1B**. These differences, introduced in the simulation model thought the spectral bands features, lead to significantly more accurate predictions than using averaged values in a single band approach, making the model capable to predict and explain the discrepancies in experimental results obtained with the solar simulator and natural sunlight. This effect is due to the fact that the emission of the solar spectrum is higher in the band between 320 and 350 nm , in which the TiO_2 has a much higher absorption coefficient, and compensates the lowest emission of the solar spectrum in the range of 370 – 400 nm , in which TiO_2 has a low absorption coefficient. This causes a better exploitation of sunlight. As shown in **Fig. 7**, for 16.4 W m^{-2} averaged emission of the xenon lamp, 207 mW are absorbed. In contrast, for 16.2 W m^{-2} of solar incident radiation, the value of energy absorbed increases up to 251 mW , resulting in a higher activity for the same catalyst concentration.

Finally, **Fig. 8** shows the comparison of the experimental reaction rates obtained in all the reactions (including artificial and solar light) with those calculated by the model. It is important to remark, that this is not a fit of the experimental data, but a prediction based on a kinetic model previously developed at laboratory scale under differential irradiation conditions. As it can be observed in the figure, data are properly distributed along the diagonal line, being the value of normalized root mean square error (NMRSE) of 14.5% .

5. Conclusions

The proposed global modelling methodology was proven to be accurate in the prediction of degradation capability of a solar photoreactor, with a global error value below a 15% for all the reaction conditions studied. The utility of obtained intrinsic kinetic parameters for predictive reactor design has been confirmed in the modelling of a reactor with different geometry and light source. The use of a spectral bands emission/absorption model allows to improve significantly the predictions, and also explain the differences observed in the photocatalytic activity using the solar simulator and natural sunlight under equivalent irradiance values.

The possibility of coupling the solar vector with rigorous calculations of the radiative transfer equation using the discrete ordinate method constitutes a promising tool for the modelling of photocatalytic reactors illuminated with solar or artificial light and represents a significant advance towards the application of this technology at large scale. We considered that the present work opens new routes in the modelling of solar photocatalytic reactors, showing how CFD simulations can be used as a valuable tool for the predictive design of systems operating with natural sunlight.

Acknowledgements

This Special Issue is dedicated to honour the retirement of Prof. César Pulgarín at the Swiss Federal Institute of Technology (EPFL, Switzerland), a key figure in the area of Catalytic Advanced Oxidation Processes and inspiration for the authors in the field of solar photocatalytic disinfection. The authors gratefully acknowledge the financial support of the Spanish State Research Agency (AEI) and the Spanish Ministry of Economy and Competitiveness (MINECO) through the project WATER4FOOD (CTQ2014-54563-C3-1-R) and Comunidad de Madrid through the program REMTAVARES (S2013/MAE-2716). Cintia Casado also acknowledges MINECO for the FPI grant (BES-2012-056661).

References

[1] D. Spasiano, R. Marotta, S. Malato, P. Fernandez-Ibañez, I. Di Somma, Solar photocatalysis: materials, reactors, some commercial, and pre-industrialized applications. A comprehensive approach, *Appl. Catal. B Environ.* 170–171 (2015) 90–123, <https://doi.org/10.1016/j.apcatb.2014.12.050>.

[2] D.D. Dionysiou, G. Li Puma, J. Ye, J. Schneider, D. Bahnemann, Chapter 4. Solar photocatalysis: fundamentals, reactors and applications, in: J. Marugán, M.J. López-Muñoz, P. Fernández-Ibañez, Sixto Malato (Eds.), *Photocatalysis: Applications, 2016*, pp. 92–129 ISBN: 978-1-78262-041-9, in:.

[3] M. Tanveer, G. Tezcanli Guyer, Solar assisted photo degradation of wastewater by compound parabolic collectors: review of design and operational parameters, *Renew. Sustain. Energy Rev.* 24 (2013) 534–543, <https://doi.org/10.1016/j.rser.2013.03.053>.

[4] C. Casado, J. Marugán, R. Timmers, M. Muñoz, R. van Grieken, Comprehensive multiphysics modeling of photocatalytic processes by computational fluid dynamics based on intrinsic kinetic parameters determined in a differential photoreactor, *Chem. Eng. J.* 310 (2017) 368–380, <https://doi.org/10.1016/j.cej.2016.07.081>.

[5] A. Castedo, I. Uriz, L. Soler, L.M. Gandía, J. Llorca, Kinetic analysis and CFD simulations of the photocatalytic production of hydrogen in silicone microreactors from water-ethanol mixtures, *Appl. Catal. B Environ.* 203 (2017) 210–217, <https://doi.org/10.1016/j.apcatb.2016.10.022>.

[6] C. Passalá, O. Alfano, R. Brandi, Integral design methodology of photocatalytic reactors for air pollution remediation, *Molecules* 22 (2017) 945, <https://doi.org/10.3390/molecules22060945>.

[7] K. Nakahara, T. Yamaguchi, E. Lim, K. Ito, Computational fluid dynamics modeling and parameterization of the visible light photocatalytic oxidation process of toluene for indoor building material, *Sustain. Cities Soc.* 35 (2017) 298–308, <https://doi.org/10.1016/j.scs.2017.08.020>.

[8] J. Colina-Márquez, F. Machuca-Martínez, G.L. Puma, Radiation absorption and optimization of solar photocatalytic reactors for environmental applications, *Environ. Sci. Technol.* 44 (2010) 5112–5120, <https://doi.org/10.1021/es100130h>.

[9] S. Malato Rodríguez, J. Blanco Gálvez, M.I. Maldonado Rubio, P. Fernández Ibáñez, D. Alarcón Padilla, M. Collares Pereira, J. Farinha Mendes, J. Correia de Oliveira, Engineering of solar photocatalytic collectors, *Sol. Energy* 77 (2004) 513–524, <https://doi.org/10.1016/j.solener.2004.03.020>.

[10] F. Colina-Marquez, J.A. Lopez-Vasquez, A.F. Machuca-Martinez, Modeling of direct solar radiation in a compound parabolic collector (CPC) with the ray tracing technique, *Dyna* 77 (163) (2010) 132–140.

[11] D. Robert, S. Malato, Solar photocatalysis: a clean process for water detoxification, *Sci. Total Environ.* 291 (2002) 85–97, [https://doi.org/10.1016/S0048-9697\(01\)01094-4](https://doi.org/10.1016/S0048-9697(01)01094-4).

[12] C.A. Arancibia-Bulnes, S.A. Cuevas, Modeling of the radiation field in a parabolic trough solar photocatalytic reactor, *Sol. Energy* 76 (2004) 615–622, <https://doi.org/10.1016/j.solener.2003.12.001>.

[13] J. Colina-Márquez, F. Machuca-Martínez, G. Li Puma, Photocatalytic mineralization of commercial herbicides in a pilot-scale solar CPC reactor: photoreactor modeling and reaction kinetics constants independent of radiation field, *Environ. Sci. Technol.* 43 (2009) 8953–8960, <https://doi.org/10.1021/es902004b>.

[14] Y. Ren, L. Zhao, D. Jing, L. Guo, Investigation and modeling of CPC based tubular photocatalytic reactor for scaled-up hydrogen production, *Int. J. Hydrogen Energy* 41 (2016) 16019–16031, <https://doi.org/10.1016/j.ijhydene.2016.04.225>.

[15] K.K. Philippe, R. Timmers, R. van Grieken, J. Marugán, Photocatalytic disinfection and removal of emerging pollutants from effluents of biological wastewater treatments, using a newly developed large-scale solar simulator, *Ind. Eng. Chem. Res.* 55 (2016) 2952–2958, <https://doi.org/10.1021/acs.iecr.5b04927>.

[16] L. Sun, J.R. Bolton, Determination of the quantum yield for the photochemical generation of hydroxyl radicals in TiO_2 suspensions, *J. Phys. Chem.* 100 (1996) 4127–4134, <https://doi.org/10.1021/jp9505800>.

[17] A. Manassero, M.L. Saturi, O.M. Alfano, Evaluation of UV and visible light activity of TiO_2 catalysts for water remediation, *Chem. Eng. J.* 225 (2013) 378–386, <https://doi.org/10.1016/j.cej.2013.03.097>.

[18] Y. Yang, Q. Wei, H. Liu, L. Zhao, Optimization of the radiation absorption for a scaled-up photocatalytic hydrogen production system, *Sol. Energy* 160 (2018) 168–177, <https://doi.org/10.1016/J.SOLENER.2017.11.068>.

[19] N. Qi, H. Zhang, B. Jin, K. Zhang, CFD modelling of hydrodynamics and degradation kinetics in an annular slurry photocatalytic reactor for wastewater treatment, *Chem. Eng. J.* 172 (2011) 84–95, <https://doi.org/10.1016/j.cej.2011.05.068>.

[20] National Renewable Energy Laboratory, Solar Position Algorithm| NREL, (2019) <http://www.nrel.gov/mide/solpos.spa.html>.

[21] Á. García-Gil, C. Casado, C. Pablos, J. Marugán, Novel procedure for the numerical simulation of solar water disinfection processes in flow reactors, *Chem. Eng. J.* (2019), <https://doi.org/10.1016/j.cej.2018.10.131>.

[22] Y. Boyjoo, M. Ang, V. Pareek, Some aspects of photocatalytic reactor modeling using computational fluid dynamics, *Chem. Eng. Sci.* 101 (2013) 764–784, <https://doi.org/10.1016/j.ces.2013.06.035>.

[23] ANSYS®, ANSYS User and Theory Guide, Release 14.5, in: ANSYS Fluent, Cecil Townsh, (2012).

[24] B.E. Launder, D.B. Spalding, The numerical computation of turbulent flows, *Comput. Methods Appl. Mech. Eng.* 3 (1974) 269–289, [https://doi.org/10.1016/0045-7825\(74\)90029-2](https://doi.org/10.1016/0045-7825(74)90029-2).

[25] S. Malato, P. Fernández-Ibáñez, M.I. Maldonado, J. Blanco, W. Gernjak, Decontamination and disinfection of water by solar photocatalysis: Recent overview and trends, *Catal. Today* 147 (2009) 1–59, <https://doi.org/10.1016/j.cattod.2009.06.018>.

[26] C. Guillard, J. Disdier, C. Monnet, J. Dussaud, S. Malato, J. Blanco, M.I. Maldonado, J.-M. Herrmann, Solar efficiency of a new deposited titania photocatalyst: chlorophenol, pesticide and dye removal applications, *Appl. Catal. B Environ.* 46 (2003) 319–332, [https://doi.org/10.1016/S0926-3373\(03\)00264-9](https://doi.org/10.1016/S0926-3373(03)00264-9).

[27] C. Casado, R. Timmers, A. Sergejevs, C.T. Clarke, D.W.E. Allsopp, C.R. Bowen, R. van Grieken, J. Marugán, Design and validation of a LED-based high intensity photocatalytic reactor for quantifying activity measurements, *Chem. Eng. J.* 327 (2017) 1043–1055, <https://doi.org/10.1016/J.CEJ.2017.06.167>.

[28] M. Martín-Sómer, B. Vega, C. Pablos, R. van Grieken, J. Marugán, Wavelength dependence of the efficiency of photocatalytic processes for water treatment, *Appl. Catal. B Environ.* 221 (2018) 258–265, <https://doi.org/10.1016/J.APCATB.2017.09.032>.